Transport across a bathymetric interface in quasi-two-dimensional flow

Lei Fang and Nicholas T. Ouellette*
Department of Civil and Environmental Engineering, Stanford University, Stanford, California 94305, USA

(Received 4 February 2019; published 3 June 2019)

Geophysical flows are often approximated as being two-dimensional on large scales due to their high aspect ratios. Two-dimensional flows in turn are well known to be prone to producing coherent structures that impact their mixing and transport. However, real geophysical flows are not exactly two-dimensional, in that they typically have nonuniform bathymetry that may also affect mixing. We study the interplay of quasi-two-dimensionality, nonuniform bathymetry, and lateral transport via laboratory experiments in an electromagnetically stirred thin-layer flow that is weakly turbulent. We find that spatial variations in bathymetry lead to laterally coexistent zones with different levels of turbulence, and we investigate the transport across the interface dividing these zones using an approach based on transfer operators. We find that this transport is asymmetric and that fluid elements cross from low turbulence to high turbulence via directed advection but from high to low turbulence via random eddying motion. Our results may have implications for understanding geophysical flows where lateral transport is suppressed, such as ocean dead zones.

DOI: 10.1103/PhysRevFluids.4.064501

I. INTRODUCTION

Geophysical flows such as those in the ocean and atmosphere can often be well approximated as two-dimensional (2D) on large scales. This reduced dimensionality has significant dynamical consequences, such as an inverse turbulent energy cascade [1–3], the introduction of an infinite number of new (inviscidly) conserved quantities [4], and a strong tendency to generate coherent structures [5] that can be linked to mixing and transport [6,7]. There has thus been a significant amount of research done on 2D flows over the past few decades [4], with the connection to geophysical flow often cited as motivation.

There are key features in real geophysical flows, however, that are not captured by a purely 2D approximation. In particular, flows in nature are always bounded from below, and the shape and structure of this bottom boundary can impact the lateral dynamics of the flow when it is shallow enough. Such bathymetric control can be particularly relevant in the coastal ocean, given the rapid horizontal variation of depth at, e.g., continental shelf breaks [8]. This dependence on the shape of the bottom can lead to lateral variations of the effective forcing of the surface layer of the ocean, since shallower sections may be more damped by interactions with the bottom, which in turn can cause variations in turbulence intensity and mixing. Such lateral variations have been implicated in the formation and dynamics of ocean dead zones [9–11], as transport may be suppressed asymmetrically across the interface separating two turbulent flows of differing strengths.

Here we make progress toward understanding the transport between flows with different degrees of turbulence using controlled laboratory experiments in a quasi-2D, weakly turbulent flow. By spatially varying the flow depth, we create two contiguous regions with different Reynolds numbers.

*nto@stanford.edu

We show that even though fluid can mix across these two regions, transport between the two is suppressed relative to what it would be in a homogeneously forced system. Using a transfer-operator framework, we describe this reduced transport in terms of a "porous" transport barrier separating the two regions. Additionally, we show that the suppression of transport is not symmetric; rather, fluid elements preferentially cross from the more turbulent side to the less turbulent side. The nature of the crossing is also different for those fluid elements that cross from less to more turbulent and more to less turbulent. In the former case, the process is one of direct advection; but in the latter, the process is more diffusive. Our results have implications for further understanding the processes by which energy, mass, and momentum are mixed in situations where flows of different turbulence levels are coexistent.

We begin by presenting a description of our experimental setup in Sec. II A and the transfer-operator framework in Sec. II B. In Sec. III we discuss our results, including the presence of a porous transport barrier and the asymmetric transport through this barrier. Finally, we summarize our results and discuss their implications in Sec. IV.

II. Methodology

A. Experimental details

To create a quasi-2D flow in the laboratory, we use an electromagnetically driven thin-layer experimental setup. As we have presented elsewhere in detail [12–15], our apparatus consists of a thin layer of an electrolytic fluid with lateral dimensions of 86×86 cm^2 driven by electromagnetic forces. Experiments were conducted with a 10-mm-deep layer of a solution of 14% by weight NaCl in deionized water, with a density of $\rho = 1101\,\mathrm{kg/m^3}$ and a kinematic viscosity of $\nu = 1.25 \times 10^{-6}$ m^2/s. A smooth flat glass floor coated with a hydrophobic wax supports the electrolyte, and the glass floor is painted black on the underside to improve imaging quality. An additional 5 mm of fresh water is floated above the electrolyte to create a miscible density interface that defines the horizontal plane of the flow.

Under the glass floor, an array of 34×34 permanent magnets with diameters of 12.7 mm, thicknesses of 3.2 mm, and center-to-center spacings of 25.4 mm is placed to generate a vertical magnetic field in the apparatus. The strength of each magnet is roughly 600 gauss on its surface, and the magnets are arranged in stripes of alternating polarity. A DC electric current of up to 3.30 A is passed laterally through the electrolyte via a pair of copper electrodes. The orthogonal current density and magnetic field produce a Lorentz body force on the fluid. This force is large enough to produce complex spatiotemporal dynamics and weak turbulence, but not so large as to drive significant out-of-plane motions [14]. We define an in-plane Reynolds number $\mathrm{Re} = u' L_m/\nu$, where u' is the in-plane root-mean-square velocity and L_m is the magnet spacing, as a nondimensionalization of the strength of the forcing. In addition to the turbulent fluctuations, the periodic layout of the magnets generates a weak mean flow consisting of shear bands of alternating sign.

The flow is measured using particle-tracking velocimetry [14,16]. We seed the electrolyte with fluorescent polystyrene tracer particles with diameters of 50 μm [and thus a Stokes number of $O(10^{-4})$] that are small enough to follow the flow accurately [17]. The mass density of the tracer particles lies between that of fresh water and the electrolyte, so the tracer particles stay at the interface between the two. We illuminate the tracer particles with LED lamps and image their motion at a rate of 60 frames per second with a 4 megapixel camera. We record roughly 25 000 particles per frame in a subregion measuring 21×21 cm^2 (roughly $8L_m \times 8L_m$) in the center of the apparatus, so that we densely sample the velocity field. Although this subregion is not precisely aligned with an integer number of magnet stripes, any asymmetric effects on transport from the small residual mean flow due to the magnets appear only on very long timescales at our flow conditions [18]. We finally combine these discrete samples into a 2D velocity field by projecting them onto a basis of stream-function eigenmodes [14].

To generate regions of the flow with different turbulence intensities, we place black polyvinyl chloride (PVC) plates with thicknesses ranging from 3 to 5 mm and lateral dimensions of 30×30 cm^2 on the glass floor in part of the flow domain. The PVC plates are fully submerged in the electrolyte, so that the flow above the plates is still driven, and they are placed such that half of the camera field of view is filled with fluid that lies over the plate and half with fluid that lies over the glass floor. For the data shown here, the plate was placed parallel to the magnet stripes (and therefore parallel to the mean-flow shear bands); however, we also tested other orientations, including perpendicular to the stripe direction and at 45°, with no significant changes to our results. Given the no-slip condition on the bottom boundary, there is a vertical velocity gradient in the flow; and since the velocity must go to zero over a shorter distance above the PVC plate, the resulting bottom drag on the fluid is larger there. In addition, the volume of driven fluid is smaller over the plate, since the interface between the salt water and fresh water does not change. Thus, the in-plane Reynolds number over the plate is smaller than that over the glass floor even for the same electric currents. Nevertheless, the flow remains quasi-2D in both cases, given that nearly all of the kinetic energy is associated with the in-plane motion [14]. In the experiments we describe here, the Reynolds number over the glass floor is maintained at roughly 200, while over the plates it drops as low as 36.

B. Transfer-operator-based partitioning

Our goal in this work is to assess the mixing and transport between two regions of the flow with distinct forcing. There are, of course, many ways to quantify mixing. Here we will primarily use an approach based on transfer operators, as it allows us to make a relatively simple characterization of the mixing properties and can reveal permeable but not unimportant impediments to mixing. We have previously described the specifics of our implementation of transfer operators [15]; here, therefore, we only briefly review the key ideas.

A transfer operator maps a density initially located in some region of the flow domain X to a (possibly) different region Y. To estimate the transfer operator, we follow Froyland *et al.* [19] and first break up the initial domain X into subsets B_i and the final domain Y into subsets C_j. The transfer operator can then be approximated as

$$\boldsymbol{P}^{(\tau)}(t)_{i,j} = \frac{l(B_i \cap \Phi(C_j, t+\tau, -\tau))}{l(B_i)}, \tag{1}$$

where $\Phi(\mathbf{z}, t, \tau)$ is the flow map that gives the location of a fluid element that was at position $\mathbf{z}$ at time t at a time $t+\tau$, and l is a normalized volume measure. Hence, $\boldsymbol{P}^{(\tau)}(t)_{i,j}$ is a row-stochastic matrix that encodes the probability that a fluid element initially in B_i at time t will be found in C_j at time $t+\tau$.

Here we estimate the transfer operator by breaking our domain into 25×25 boxes, corresponding to the B_i in Eq. (1). Since we are interested in coherent transport within the domain, the set C_j is taken to be the same as the set B_i. Both the domain and the boxes have unit aspect ratio to avoid possible biases. In each box, $N_p = 225$ virtual Lagrangian points are seeded uniformly. The Lagrangian points are integrated forward in time using a second-order Runge-Kutta scheme, with the advecting velocity taken from the measured flow fields [17]. We varied the number of boxes and number of particles in each box over a reasonable range, with no significant changes; for example, we tested box layouts ranging from 16×16 to 50×50. We find that 25×25 boxes with each box containing 225 virtual Lagrangian points is a good compromise between accuracy and resolution [15].

After estimating the transfer operator, we apply the flow partition algorithm of Froyland *et al.* [19] to split the flow domain into sets using the singular vector corresponding to the second-largest singular value of the transfer operator σ_2, as it is guaranteed by the Perron-Frobenius and Courant-Fischer theorems to produce the maximally coherent sets [19,20]. Note that we modify the algorithm

detailed in Froyland *et al.* [19] somewhat to handle the open boundaries of our flow domain (as is typical for experimental or observational data), as we have described previously [15].

The level of coherence of the two sets is indicated by σ_2, since the largest singular value σ_1 is always unity and simply represents conservation of mass; thus, we require σ_2 to be larger than a threshold (0.8, here) to ensure that the flow domain can be reasonably partitioned. Varying this threshold over a reasonable range does not change our results [15], and the typical magnitudes of σ_2 can be seen in Fig. 2. But the value of σ_2 alone does not directly tell us how confident we are that the partition returned by the algorithm is the best one as opposed to some other partition, such as that based on the third singular value σ_3. If σ_2 is significantly larger than σ_3, we can assert that a partition based on the third singular vector will be significantly inferior. On the other hand, if σ_2 and σ_3 are close in magnitude, the confidence in the partition is much lower, because noise or uncertainty could potentially have changed the ordering of the singular values. To ensure that the partitioning is meaningful, we therefore also require the spectral gap between σ_2 and σ_3 to be significant. Hence, we enforce two criteria in reporting transfer-operator-based flow partitions: that (1) the second singular value σ_2 must be larger than a threshold so that the partition is sufficiently coherent and therefore meaningful, and that (2) the spectral gap σ_2/σ_3 between the second and third singular values should also be large so that we have confidence in the partition as opposed to a different partition.

The transfer operator, and therefore the corresponding flow partition, is also dependent on the timescale τ over which we allow the flow to evolve. This timescale is a free parameter and encodes the time span over which we will look for coherent transport. In principle, it ought to be determined by the flow physics itself; however, the relevant timescales of the flow are not always known *a priori*. Thus, we previously suggested that it is useful to track the evolution of the singular values of the transfer operator as τ is increased [15]; and, typically, one observes that the singular value ratio σ_2/σ_3 displays rapid jumps at some values of τ. These values indicate important dynamical timescales of the flow, since on these timescales the confidence in the flow partition dramatically increases and it becomes more meaningful.

Finally, we note that the raw singular vectors of the transfer operator produce spatial values that are continuously distributed. We will refer to such a spatial map (such as the one shown in the top panels in Fig. 3 below) as a "fuzzy" partition. These values give an estimate of the likelihood that a particular spatial location belongs to one set or the other; values close to 1 and -1 are quite likely to belong to one set, while those closer to 0 are less certain [15,19]. It is often useful, however, to binarize the partition, which we do here simply by choosing a binarization threshold so that each of the coherent sets contains about half of the domain; here we simply choose a threshold of 0.

III. RESULTS

As discussed above, our goal is to study the mixing and transport between different regions in the flow with different depths, because the in-plane flows in these regions have different levels of turbulence, as reflected in distinct in-plane Reynolds numbers. We studied regions with Reynolds number ratios ranging from 1.26 to 5, with similar results; below we show specific results for the case of a Reynolds number ratio of 1.26 (with individual Reynolds numbers of 237 and 188). We begin by confirming the suppressed mixing across the interface between the two regions, which we describe as a "porous" transport barrier. We then describe asymmetries in the transport, since moving from high to low Reynolds number is not the same as moving from low to high.

A. Detecting porous transport barriers

Since their introduction as tools for locating so-called Lagrangian coherent structures [6], finite-time Lyapunov exponents (FTLEs) have become standard tools for studying transport in complex flows. FTLEs are typically obtained by measuring the eigenvalues of the right Cauchy-Green strain tensor, which can be computed by taking the inner product of the gradient of the flow map with itself

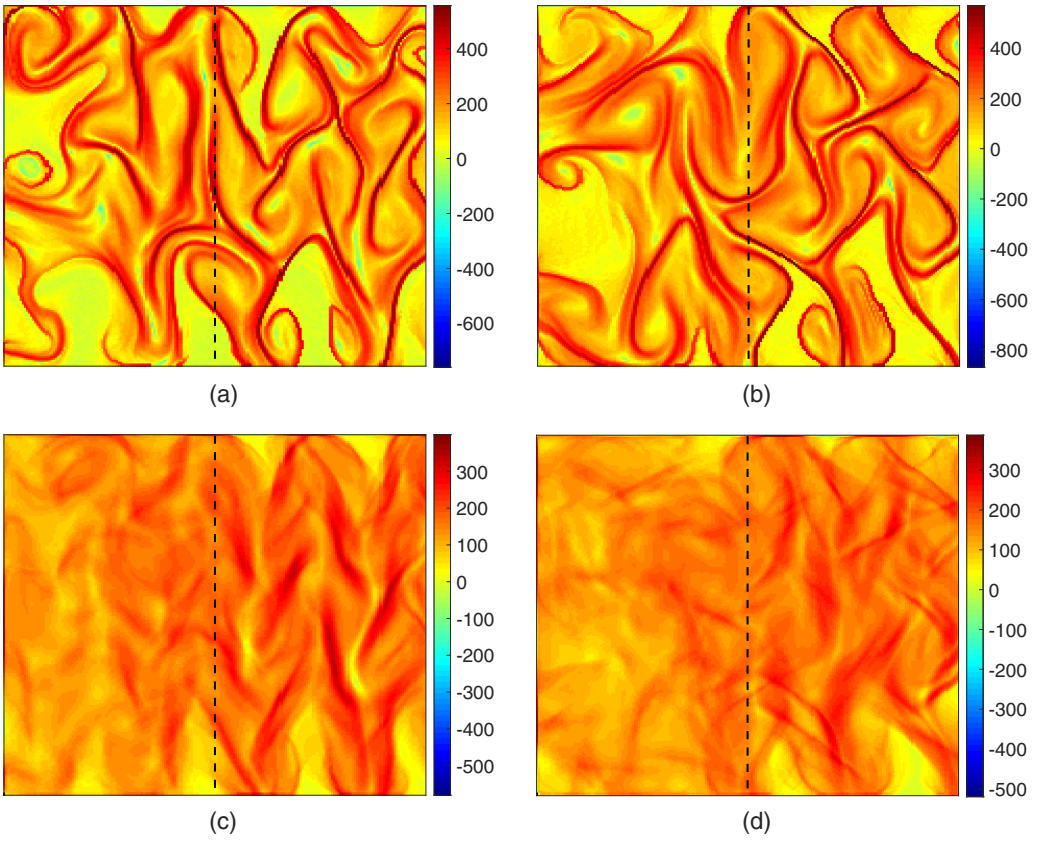

FIG. 1. (a) Instantaneous forward finite-time Lyapunov exponent (FTLE) field computed for an integration time of $2.5T_L$, where $T_L = L_m/u'$ is the eddy turnover time associated with the forcing. The dashed line shows the location of the bathymetric step; the low Reynolds number side is on the left of the figure, and the high Reynolds number side is on the right. (b) Backward FTLE field, computed for the same integration time. (c) Temporally averaged forward FTLE field. (d) Temporally averaged backward FTLE field. All FTLE values have been nondimensionalized by T_L, and the size of the domain shown in all cases is $8L_m \times 8L_m$ (or 21×21 cm^2).

[6]. For an in-depth discussion of FTLEs and associated Lagrangian coherent structures, we direct the reader to recent review articles in Refs. [6,7]. For our purposes here, it is sufficient to recall that sharp (codimension-one) ridges of the FTLE field are expected to indicate the presence of dynamical barriers to transport [21]. As we wish to characterize a potential suppression of transport between two regions of the flow, it stands to reason that we might expect to see a strong ridge of the FTLE field, corresponding to such a transport barrier, pinned at the interface between the high and low Reynolds number regions. Such behavior has indeed been seen previously in the oceanic context separating dead zones from the rest of the ocean, such as on the West Florida shelf [9,11].

When we measure FTLE fields such as those shown in Fig. 1, however, we see no hint of a barrier between the two regions. This is true whether we look at either the forward- or backward-time FTLEs, whether we average these fields over time [18], or the Reynolds number ratio between the two regions. The patterns seen in the averaged FTLE fields are due to the arrangement of the magnets, as we have previously shown [18]; when averaged over long times, the FTLEs are sensitive to the (weak) mean flow. These results tell us that even though the mixing between the two regions may be suppressed, there is no true barrier between them: fluid elements may still cross from one region to the other.

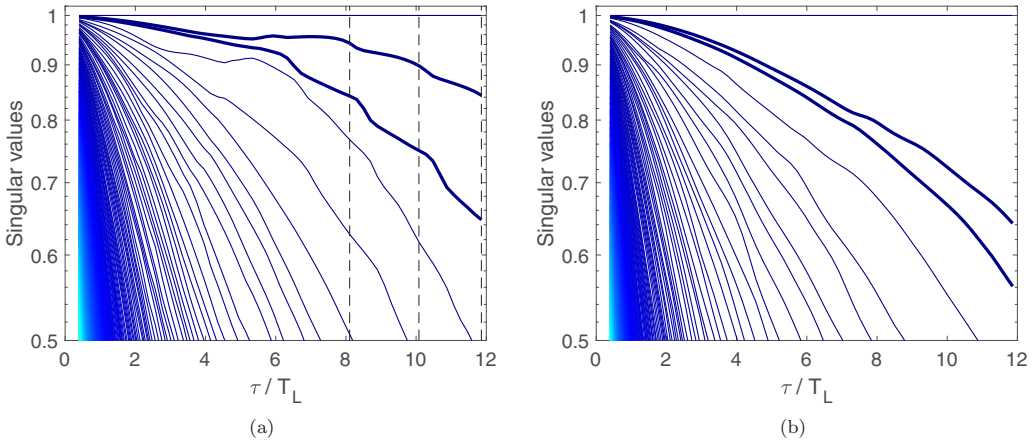

FIG. 2. Evolution of the transfer operator singular values as a function of the integration time τ over which the transfer operator is computed, in units of $T_L = L_m/u'$, for (a) experiments with a bathymetric step and (b) the control case of featureless bathymetry. The largest singular value is fixed at 1 by construction, but the other singular values decay with increasing τ, indicating loss of coherence. The second and third singular values σ_2 and σ_3 are plotted with thicker lines. As discussed in the text, the value of σ_2 indicates the degree of coherence of our partition, and the gap between σ_2 and σ_3 indicates our confidence in this partition. The vertical dashed lines in panel (a) show the values of τ for which partitions are shown in Fig. 3. In the control case, σ_2 decays very quickly as τ increases, indicating a rapid drop in coherence. Additionally, the spectral gap between σ_2 and σ_3 remains small for all τ, indicating low confidence.

The existence of an impermeable barrier to mixing, however, would be a very strong result, and one that perhaps should not be expected here. Instead, it is more reasonable to posit that there is instead simply a reduced tendency to mix across the interface between the two regions. To check that hypothesis, we turn to the transfer operator described above: since transfer-operator partitioning looks only for maximally coherent sets rather than impermeable boundaries, it may reveal the transport modulation we seek even though the FTLEs do not.

In Fig. 2(a) we plot the singular values of the transfer operator for different mapping times τ, ensemble-averaged over 30 different realizations of the flow separated by at least one correlation time of the flow field, ensuring their statistical independence. We note that all of our transfer-operator results are similarly ensemble-averaged. We find, similarly to our previous work on the effects of lateral boundaries (e.g., coastlines) on mixing [15], that each of the singular values decays with τ, but at different rates. In particular, the larger singular values decay more slowly, indicating that the singular vectors associated with them correspond to fairly coherent sets. As τ increases, the spectral gap between the second and third singular values, which indicates the confidence with which we can assert that the second singular vector identifies the most coherent partition of the flow, also increases, while the second singular value remains high. These results indicate that there is indeed a meaningful binary partitioning of the flow that can be determined, even though the FTLE fields did not indicate the presence of an impermeable transport barrier.

To ensure that this result is not an artifact of the partitioning algorithm, we also tested a control case where we applied the algorithm to a flow with a uniform bottom boundary (and thus no distinct regions). The transfer-operator singular values for this control case are shown in Fig. 2(b). Unlike the situation shown in Fig. 2(a), the second singular value decreases rapidly, indicating that the best binary partition of the flow is not very coherent, and the spectral gap between the second and third singular values is small, indicating that there is little confidence in this best binary partition compared to other possible partitions. These results are borne out by looking at the coherent sets themselves for the control case, which are spatially unstructured. Thus, the case of interest with

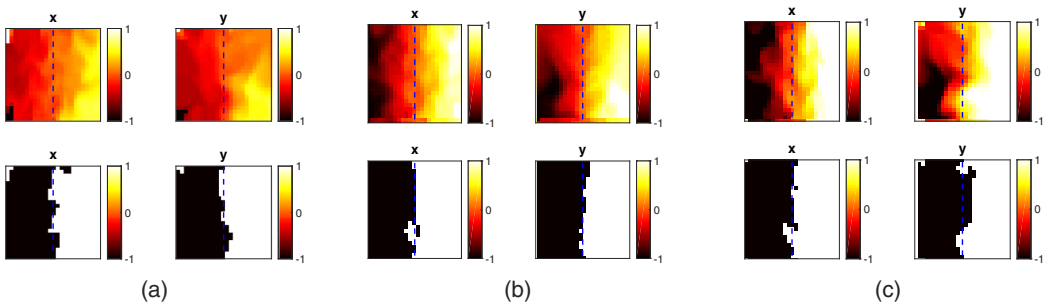

FIG. 3. Flow partitions for (a) $\tau = 8T_L$, (b) $10T_L$, and (c) $12T_L$ for the case with variable bathymetry. For each value of τ, the top two panels show the singular vectors X (at the initial time) and Y (at the final time), while the bottom two panels show the same data but binarized following the work of Froyland *et al.* [19]. The dashed lines show the location of the bathymetric step; the low Reynolds number side is on the left, and the high Reynolds number side is on the right. The size of the domain shown in all cases is $8L_m \times 8L_m$ (or 21×21 cm^2). The values of the second singular value σ_2 and the ratio σ_2/σ_3 are (a) 0.94 and 1.119, (b) 0.90 and 1.198, and (c) 0.84 and 1.304.

variable bathymetry is both qualitatively and quantitatively distinct from the homogeneous control case. Thus, we conclude that the partition picked out by the transfer operator is not simply due to noise or the geometry of the domain.

Having established that the partition is likely to be meaningful, we visualize it by plotting the identified coherent sets in Fig. 3. We show results for three values of τ: $8T_L$, $10T_L$, and $12T_L$, where $T_L = L_m/u'$ is the eddy turnover timescale associated with the flow forcing. These values were chosen by examining the evolution of the spectral gap σ_2/σ_3 with τ; at each of these times, a rapid increase in the spectral gap was seen, indicating an increase in the confidence of partitioning [15]. For each of these cases, we show both the fuzzy and binary partitions at both the initial and final times (that is, the initial shapes of the coherent sets and their final shapes a time τ later). We also indicate the position of the bathymetric step. The interface between the two coherent sets clearly lies on this step. For the control case with no bathymetry, the partitioning algorithm simply splits the domain in half along the longest axis of the measurement domain (that is, along the diagonal), with fuzzy partition values near 0 indicating low confidence. Thus, we conclude that transport is indeed meaningfully reduced between the two regions with different bathymetries: more than 90% of fluid elements initially on one side of the barrier do not cross it. However, transport is not completely suppressed, as the interface is not apparent from FTLE fields and some fluid elements do cross. For that reason, we refer to the interface between these two turbulent regions as a "porous" transport barrier.

B. Asymmetric transport

Now that we have demonstrated the existence of a porous transport barrier between the two regions of the flow with different bathymetries and therefore different Reynolds numbers, we investigate the properties of those fluid elements that are able to cross the barrier as compared to those that do not. Additionally, we separate those fluid elements that cross from the low Reynolds number side to the high Reynolds number side from those that cross from high to low, since the transport need not be symmetric given that there is a substantial amount of the full apparatus that we do not measure and thus that our measurement domain is effectively an open flow.

More specifically, we seeded 256 640 virtual fluid elements at specified initial locations on both sides of the porous transport barrier and integrate their positions forward in time using the measured velocity fields, just as we did to compute the transfer operator and the FTLE fields. From this ensemble, we pick out four classes of trajectories: those that remain in the low Reynolds number

region, those that remain in the high Reynolds number region, those that cross from the low to the high Reynolds number side, and those that cross from the high to the low Reynolds number side. Using these data, we first verify that the transport we observed across the barrier is indeed asymmetric: the ratio of the mass flux from high to low Reynolds number to low to high Reynolds number is about 1.6. To gain more insight, we then consider the statistics of the kinetic energy and vorticity for these classes of fluid elements conditioned on their initial distance from the barrier. Finally, we also consider the initial direction of motion of the fluid elements, expressed as the angle of their velocity vector with respect to the direction normal to the barrier.

We first consider the kinetic energy statistics. In Fig. 4 we show the probability density functions (PDFs) of kinetic energy for fluid elements in the four classes described above for different initial distances to the barrier. From these data, one can observe that fluid elements that move from the low Reynolds number side of the barrier to the high Reynolds number side tend to have larger kinetic energy, particularly when they are initially further from the barrier. This result is compatible with a simple explanation in terms of smoothness of the velocity field. Once a fluid element is on the high Reynolds number side, its kinetic energy must be (on average) larger, since the typical length scales and viscosities are fixed on each side of the barrier; thus, those fluid elements on the low side that already have higher than average kinetic energy need to accelerate less to cross the barrier. What is perhaps less obvious is that the same trend, albeit more weakly, is also observed for fluid elements that cross from high to low Reynolds number as compared with those that remain on the high side. Such fluid elements must then decelerate rapidly once they cross the barrier to preserve the stationarity of the flow. Thus, studying the kinetic energy alone is not sufficient to understand the asymmetric transport we see.

Because in 2D flows the enstrophy, like the kinetic energy, is an inviscid invariant along fluid-element trajectories and therefore contains significant dynamical information, we also measured the statistics of the magnitude of the vorticity for our four classes of fluid elements, as shown in Fig. 5. Here as well, there are noticeable differences between those fluid elements that cross the barrier and those that do not. Fluid elements that cross from low to high Reynolds number tend to have somewhat lower vorticity than those that do not cross, while those that cross from high to low Reynolds number tend to have somewhat higher vorticity. To summarize, in terms of their kinematics, we find that fluid elements that cross the barrier from low to high Reynolds number tend on average to have high kinetic energy but low vorticity, while those that cross from high to low Reynolds number tend to have high kinetic energy and high vorticity. Thus, we conclude that the transport across the barrier is not necessarily symmetric.

To gain more insight into the mechanics of the barrier crossing, we also measured a simple quantity: the angle between the velocity vector of a fluid element and the direction normal to the barrier at various distances from the barrier. We define the barrier normal vector to point from the high Reynolds number side to the low Reynolds number side; thus, angles ranging from 0° to 90° indicate a velocity vector with a component pointed toward the low Reynolds number side, and angles ranging from 90° to 180° indicate a velocity vector with a component pointed toward the high Reynolds number side. Because of the symmetry of the problem in the direction parallel to the boundary, we do not distinguish between clockwise and counterclockwise angles.

We show the statistics of these angles for fluid elements that cross the barrier in Fig. 6. For fluid elements that cross from low to high Reynolds number, there is a definite bias in the PDFs for velocities pointed toward the barrier, as one would expect, particularly for fluid elements fairly far from the barrier. Surprisingly, however, fluid elements that cross from high to low Reynolds number are nearly as likely to be moving *away* from the barrier as they are to be moving toward the barrier, though the mean direction is still (weakly) toward the barrier. This asymmetry combined with the results for kinetic energy and vorticity above suggests that fluid elements move from the low to high Reynolds number side by directed advection, while they move from the high to the low side via more random eddying motions. This result also gives a rationalization for why it is the higher-energy fluid elements on the high Reynolds number side that cross the barrier: those fluid elements on the high Reynolds number side with higher kinetic energies will move farther in the same amount of time

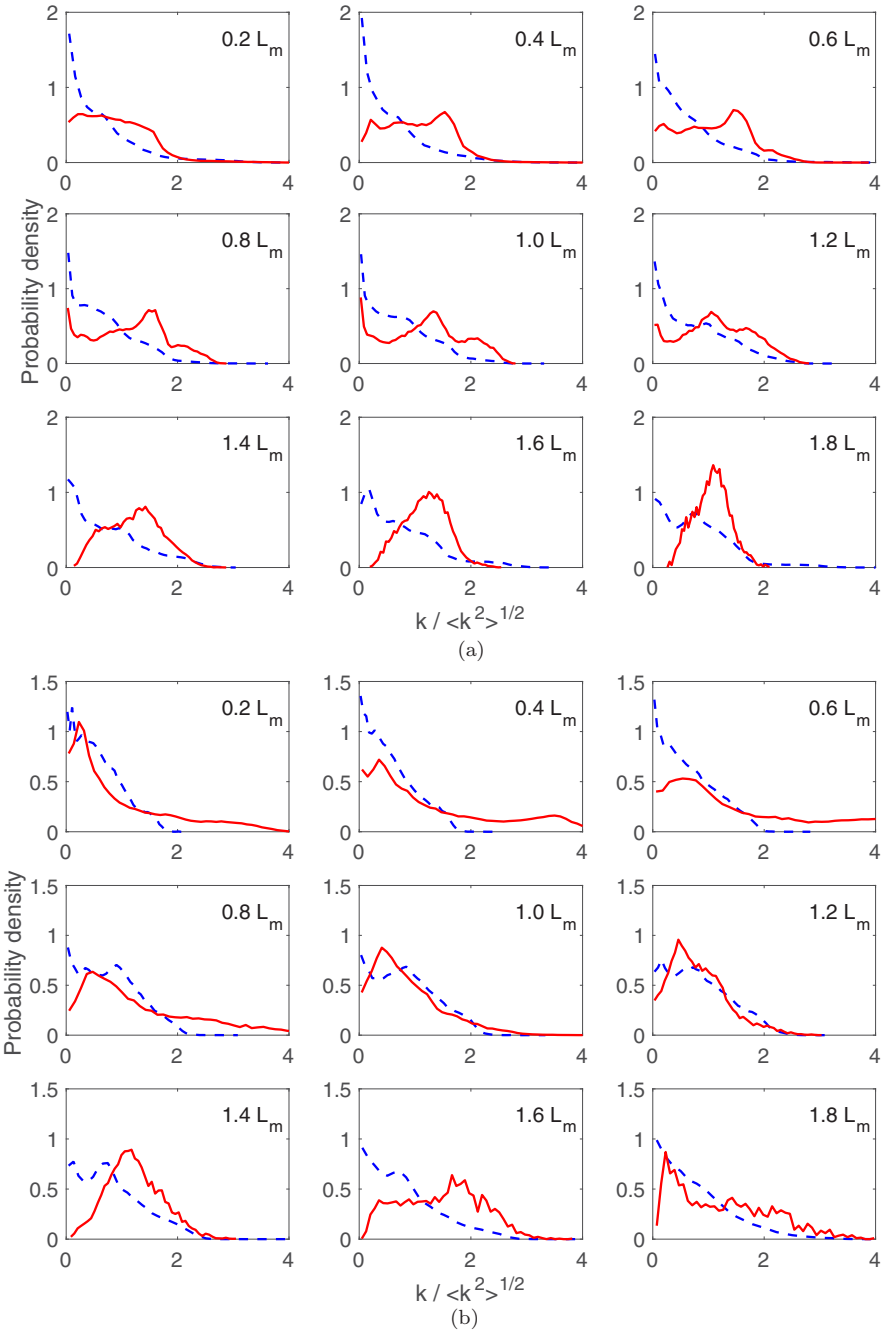

FIG. 4. Probability density functions (PDFs) of the kinetic energy k of fluid elements located at fixed distances (ranging from $0.2L_m$ to $1.8L_m$) to the bathymetric step on (a) the low Reynolds number side and (b) the high Reynolds number side. Solid lines show the statistics of fluid elements that eventually crossed the porous transport barrier, while dashed lines show the statistics of fluid elements that did not.

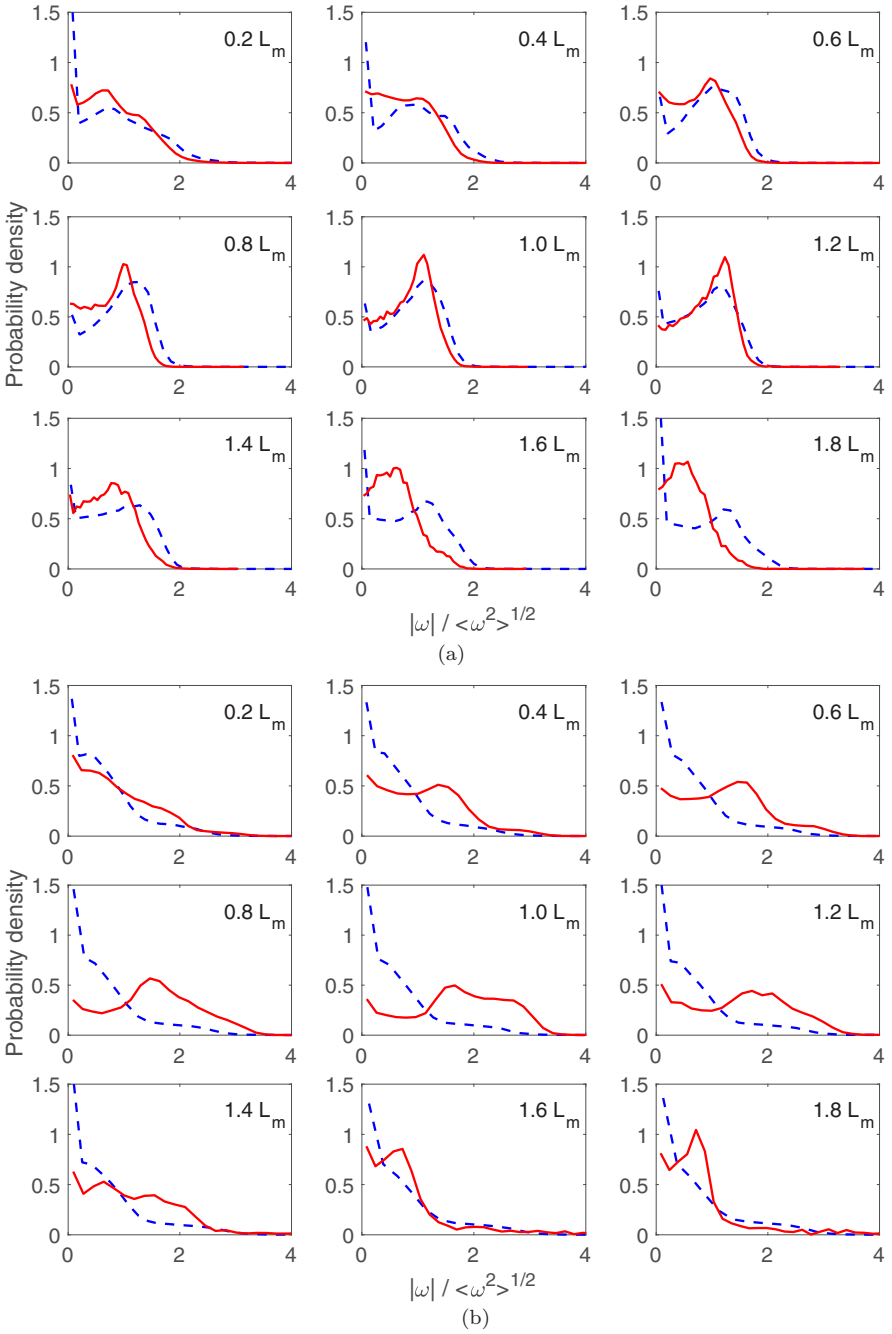

FIG. 5. PDFs of the magnitude of the vorticity $|\omega|$ of fluid elements located at fixed distances (ranging from $0.2L_m$ to $1.8L_m$) to the bathymetric step on (a) the low Reynolds number side and (b) the high Reynolds number side. Solid lines show the statistics of fluid elements that eventually crossed the porous transport barrier, while dashed lines show the statistics of fluid elements that did not.

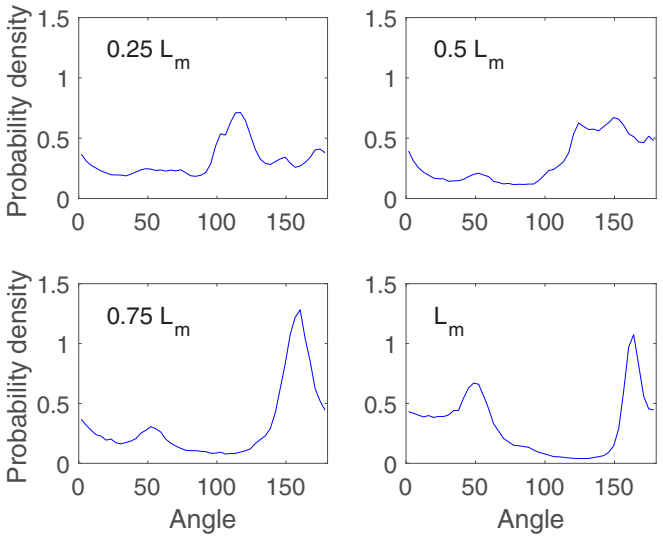

(a)

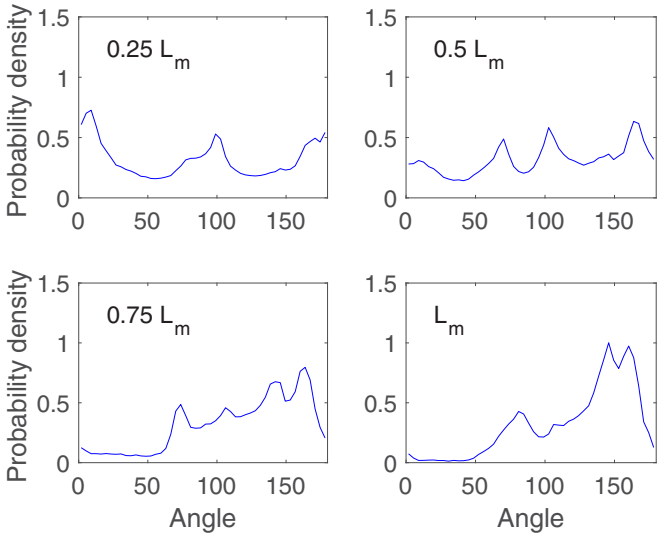

(b)

FIG. 6. PDFs of the angle between the velocity vector of fluid elements located at fixed distances to the bathymetric step and the direction normal to the step for (a) fluid elements initially on the low Reynolds number side and (b) fluid elements initially on the high Reynolds number side.

via their random motions than those with lower kinetic energy, and will therefore be more likely to encounter the barrier.

We can solidify this picture by considering the likelihood of a fluid element that started some distance away from the barrier to cross it. To do so, we measured the PDFs of the initial distance from the barrier for those fluid elements that cross it from high to low Reynolds number and from low to high Reynolds number, as shown in Fig. 7 for fluid elements integrated for a time of $2T_L$. If the crossing were random, one would expect a PDF that falls off exponentially; and, indeed, this is roughly what we find for the high to low Reynolds number case. In contrast, the PDF for the low to

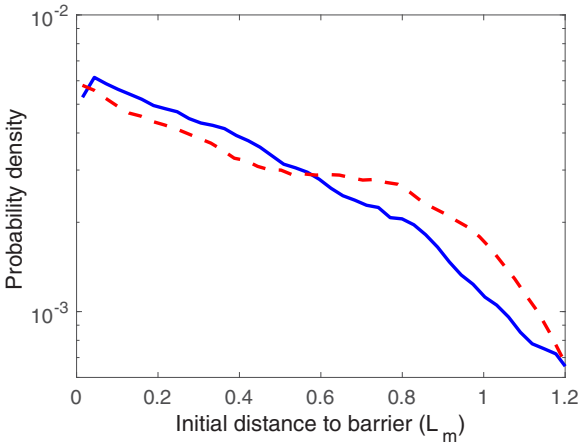

FIG. 7. PDFs of the initial distance to the barrier for fluid elements that eventually cross it (in a time less than or equal to $2T_L$) from low to high Reynolds number (dashed line) and from high to low Reynolds number (solid line).

high Reynolds crossing is not exponential except for very close to the interface. We note that there is some dependence on the integration time for these PDFs; as the integration time becomes very short, the PDFs become very similar, since not many fluid elements cross the barrier. The deviation between the PDFs grows as the integration time increases, for reasonable integration times.

IV. SUMMARY AND CONCLUSIONS

We have used a modified transfer-operator-based approach to study the coherent transport across a bathymetric interface separating two quasi-2D turbulent flows of different strength. We find evidence for a porous transport barrier at this interface, which is not apparent using an FTLE-based approach. The transport across this barrier is highly anisotropic, with preferential transport from the high Reynolds number side to the lower Reynolds number side. However, this process is roughly diffusive, while transport from the low Reynolds number side to the high Reynolds number side is more advective. We suggest that these ideas may be useful for further understanding of the origin and dynamics of ocean dead zones, as well as for the siting of coastal facilities that discharge material into the ocean and assume that it will mix [22].

Finally, although we have here focused on the effects of variable bathymetry in driving differential transport, it is likely that our qualitative results will hold for any system similar to ours with a laterally varying local Reynolds number. Future work could test this hypothesis by changing the Reynolds number spatially in different ways and studying the more general transport across such a turbulent-turbulent interface.

ACKNOWLEDGMENT

This research was supported by the U.S. National Science Foundation under Grant no. CMMI-1563489.

[1] R. H. Kraichnan, Inertial ranges in two-dimensional turbulence, Phys. Fluids **10**, 1417 (1967).
[2] C. E. Leith, Diffusion approximation for two-dimensional turbulence, Phys. Fluids **11**, 671 (1968).

[3] G. K. Batchelor, Computation of the energy spectrum in homogeneous two-dimensional turbulence, Phys. Fluids **12**, II-233 (1969).
[4] G. Boffetta and R. E. Ecke, Two-dimensional turbulence, Annu. Rev. Fluid Mech. **44**, 427 (2012).
[5] P. Tabeling, Two-dimensional turbulence: A physicist approach, Phys. Rep. **362**, 1 (2002).
[6] G. Haller, Lagrangian coherent structures, Annu. Rev. Fluid Mech. **47**, 137 (2015).
[7] S. Balasuriya, N. T. Ouellette, and I. I. Rypina, Generalized Lagrangian coherent structures, Physica D **372**, 31 (2018).
[8] T. C. Malone, T. S. Hopkins, P. G. Falkowski, and T. E. Whitledge, Production and transport of phytoplankton biomass over the continental shelf of the New York bight, Continent. Shelf Res. **1**, 305 (1983).
[9] M. J. Olascoaga, I. I. Rypina, M. G. Brown, F. J. Beron-Vera, H. Koçak, L. E. Brand, G. R. Halliwell, and L. K. Shay, Persistent transport barrier on the West Florida Shelf, Geophys. Res. Lett. **33**, L22603 (2006).
[10] R. J. Diaz and R. Rosenberg, Spreading dead zones and consequences for marine ecosystems, Science **321**, 926 (2008).
[11] M. J. Olascoaga, Isolation on the West Florida Shelf with implications for red tides and pollutant dispersal in the Gulf of Mexico, Nonlin. Proc. Geophys. **17**, 685 (2010).
[12] L. Fang and N. T. Ouellette, Multiple stages of decay in two-dimensional turbulence, Phys. Fluids **29**, 111105 (2017).
[13] Y. Liao and N. T. Ouellette, Spatial structure of spectral transport in two-dimensional flow, J. Fluid Mech. **725**, 281 (2013).
[14] D. H. Kelley and N. T. Ouellette, Onset of three-dimensionality in electromagnetically forced thin-layer flows, Phys. Fluids **23**, 045103 (2011).
[15] L. Fang and N. T. Ouellette, Influence of lateral boundaries on transport in quasi-two-dimensional flow, Chaos **28**, 023113 (2018).
[16] N. T. Ouellette, H. Xu, and E. Bodenschatz, A quantitative study of three-dimensional Lagrangian particle tracking algorithms, Exp. Fluids **40**, 301 (2006).
[17] N. T. Ouellette, P. J. J. O'Malley, and J. P. Gollub, Transport of Finite-Sized Particles in Chaotic Flow, Phys. Rev. Lett. **101**, 174504 (2008).
[18] N. T. Ouellette, C. A. R. Hogg, and Y. Liao, Correlating Lagrangian structures with forcing in two-dimensional flow, Phys. Fluids **28**, 015105 (2016).
[19] G. Froyland, N. Santitissadeekorn, and A. Monahan, Transport in time-dependent dynamical systems: Finite-time coherent sets, Chaos **20**, 043116 (2010).
[20] C. R. Horn and R. A. Johnson, *Matrix Analysis* (Cambridge University Press, Cambridge, 1990).
[21] S. C. Shadden, F. Lekien, and J. E. Marsden, Definition and properties of Lagrangian coherent structures from finite-time Lyapunov exponents in two-dimensional aperiodic flows, Physica D **212**, 271 (2005).
[22] Y. Fernández-Torquemada, J. M. Gónzalez-Correa, A. Loya, L. M. Ferrero, M. Díaz-Vadés, and J. L. Sánchez-Lizaso, Dispersion of brine discharge from seawater reverse osmosis desalination plants, Desal. Wat. Treat. **5**, 137 (2009).